ChemComm

COMMUNICATION

View Article Online
View Journal | View Issue

Cite this: *Chem. Commun.*, 2024, **60**, 14391

Received 15th October 2024,
Accepted 8th November 2024

DOI: 10.1039/d4cc05468g

rsc.li/chemcomm

Hydrazone-linked covalent organic frameworks for fluorescence detection of Hg^{2+}†

Xuefeng Wang,[a] Zhaowei Yang,[a] Lingsuo Meng,[a] Xuehui Li,[a] Hongtao Wei,[a] Jing Ning,*[a] Shitao Wang,[b] Dapeng Cao*[b] and Long Hao[a]

A hydrazone-linked COF (DvDf-C3XJ-COF) with hydrogen-bond reinforcement and abundant coordination sites was synthesized, exhibiting strong fluorescence and high sensitivity/selectivity for Hg^{2+} detection, with a detection limit of 1.65×10^{-6} M. The fluorescence quenching for Hg^{2+} is attributed to coordination interactions, which occur through a dynamic quenching process.

Heavy metals, such as mercury (Hg), not only pollute the environment but also pose significant threats to human health. Naturally present in air, water, and soil, Hg can spread widely through natural processes and human activities.[1] Hg^{2+}, in both its inorganic and organic forms, is a persistent toxic pollutant that accumulates in organisms *via* the food chain. Mercury exposure can cause serious health problems, including heart attacks, Minamata disease, and autism, by damaging the kidneys, as well as the nervous and reproductive systems.[2] However, traditional Hg^{2+} detection methods are often expensive and complex, requiring bulky equipment, which makes them unsuitable for routine use.[3] Therefore, a sensitive, selective, and straightforward method to monitor Hg^{2+} in the environment and food chain is urgently needed, for protecting human health and global resources.

Covalent organic frameworks (COFs) are a novel class of crystalline porous materials composed entirely of organic building units.[4] With their large surface area, excellent chemical stability, and permanent porosity, COFs hold great potential for various applications,[5] such as catalysis, energy storage, gas storage, sensing and separation. In particular, they show promise in chemical sensing.[6] COFs are insoluble in most organic and inorganic solvents, and this property simplifies calibration, separation, and regeneration processes. Additionally, the porous structure, combined with numerous functional sites and an extended π-conjugated system, provides a rigid and uniform framework that allows efficient analyte penetration and interaction with recognition sites, thereby enhancing detection sensitivity.[7] Compared to traditional methods, fluorescence-based COFs offer higher sensitivity and a quicker response. There have been several cases where sulfur-functionalized COFs, constructed through post-modification methods, were used for the detection of mercury ions *via* sulfur–mercury coordination. These studies have made some progress in the field of mercury detection based on COFs. However, the involvement of post-modification steps for COFs adds to the workload.[8]

In the field of fluorescence sensing, the luminescent properties of COF materials are the primary factor of interest. However, most traditional COFs are predominantly connected by imine bonds, whose rotational freedom can result in non-radiative deactivation of the excited state, leading to fluorescence quenching.[9] Therefore, the rational design of COFs with fluorescent properties that can selectively bind to Hg^{2+} has become a critical focus in current research. Studies have shown that COFs linked by hydrazone bonds are particularly favourable for enhancing fluorescence emission.[10] Moreover, the hydrazone linkage, which is rich in nitrogen and oxygen atoms, offers potential coordination sites for metal ions.[11] By carefully designing the structural units in the construction of COFs, one can develop the frameworks facilitating coordination with target analytes, thereby improving the sensitivity and selectivity of fluorescence-based detection methods.

In this study, alkoxy-containing acylhydrazide (C3XJOPr) and 2,5-divinylterephthalaldehyde (DvDf) were selected as precursors to construct a novel hydrazone-linked COF, denoted as DvDf-C3XJ-COF, *via* a Schiff base reaction. The oxygen atoms in the alkoxy groups can form hydrogen bonds with the nitrogen atoms in the hydrazone linkage. The formation of hydrogen bonds not only enhances the structural stability of

[a] *College of Chemistry and Pharmaceutical Sciences, Qingdao Agricultural University, No. 700 Changcheng Road, Qingdao 266109, P. R. China. E-mail: ningj@qau.edu.cn*
[b] *State Key Laboratory of Organic–Inorganic Composites, Beijing University of Chemical Technology, Beijing 100029, P. R. China. E-mail: caodp@mail.buct.edu.cn*

† Electronic supplementary information (ESI) available: Materials and methods, synthetic procedures, experimental details and supplementary figures. See DOI: https://doi.org/10.1039/d4cc05468g

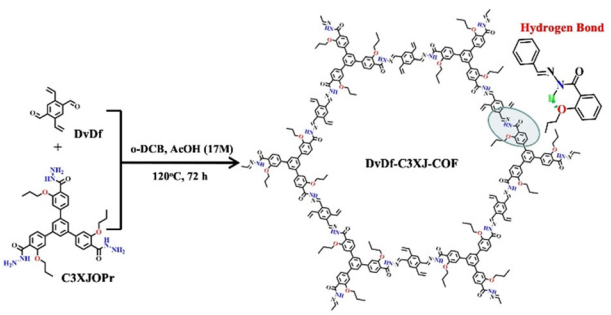

Scheme 1 A schematic illustration of the synthesis route of DvDf-C3XJ-COF, as well as the formation of hydrogen bonds.

the DvDf-C3XJ-COF but also increases the degree of conjugation, further promoting fluorescence emission. As a result, DvDf-C3XJ-COF exhibits favorable fluorescence properties in solution. The introduction of hydrazone linkages avoids the fluorescence quenching commonly observed in imine-linked COFs, while the presence of multiple N/O heteroatoms facilitates coordination with Hg^{2+}, enabling rapid fluorescent detection of Hg^{2+}. This work reports the construction of a novel fluorescent COF and its application in the rapid detection of mercury, providing new insights into the design of fluorescent COFs for sensing Hg^{2+}.

The synthesis of DvDf-C3XJ-COF was carried out by the Schiff base condensation between the building units DvDf and C3XJOPr (Scheme 1). The complete reaction details can be found in the ESI.† The formation of the hydrazone linkage within the COF framework and the condensation of monomers, were confirmed through Fourier transform infrared (FT-IR) spectroscopy (Fig. 1a). In the FT-IR spectrum of DvDf-C3XJ-COF, a characteristic vibrational band at 1621 cm^{-1} signifies the successful condensation of DvDf and C3XJOPr through the formation of –C═N– bonds. Furthermore, the $\nu_{C=O}$ band in DvDf-C3XJ-COF appears at 1667 cm^{-1}, displaying a blue shift compared to the corresponding band at 1650 cm^{-1} in the monomer C3XJOPr. This observed blue shift is likely due to the weakening of $\nu_{C=O}$ bonds influenced by neighboring imine groups, a similar phenomenon has also been observed in COF-42.[12] The crystalline structure of DvDf-C3XJ-COF was characterized through X-ray diffraction (XRD) analysis (Fig. 1b). The notable peak observed at 2.41° is associated with the (100) crystal plane, while a broader peak appearing at a higher 2θ value (approximately 25.0°) is primarily linked to π–π stacking interactions occurring between the COF layers, corresponding to the (001) plane. A comparison between the experimental XRD patterns and the simulated ones reveals that the COF adopts a layered structure featuring eclipsed (AA) stacking, with the space group classified under *P*6/*m* symmetry. (Fig. 1c). The simulated cell parameters of DvDf-C3XJ-COF are $a = b =$ 41.99 Å, $c = 3.53$ Å; $\alpha = \beta = 90°$, $\gamma = 120°$ (Table S1, ESI†). The permanent porosity of DvDf-C3XJ-COF was assessed through nitrogen (N_2) adsorption isotherms measured at 77 K (Fig. 1d). The resulting data revealed type-I isotherms, indicating the microporous structures of DvDf-C3XJ-COF. The surface area of DvDf-C3XJ-COF was analyzed by Brunauer–Emmett–Teller (BET) to be 431 $m^2\ g^{-1}$. The nonlocal density functional theory (NLDFT) analysis based on the nitrogen adsorption–desorption measurements indicated a narrow pore size distribution, with the average pore width of ~2.59 nm (Fig. 1d inset). Thermal stability of DvDf-C3XJ-COF was evaluated using thermogravimetric analysis (TGA). The TGA results demonstrate that DvDf-C3XJ-COF remains thermally stable up to 350 °C (Fig. S1, ESI†), which can be attributed to the presence of hydrazone linkages within the COF structure.[12] The PXRD patterns of DvDf-C3XJ-COF in aqueous solutions, spanning a pH range from 3 to 11, remain consistent, demonstrating its remarkable chemical stability (Fig. S2, ESI†).

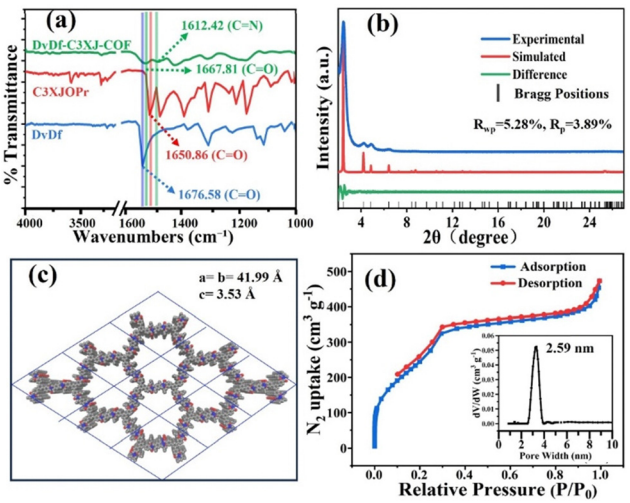

Fig. 1 (a) FT-IR spectroscopy of DvDf-C3XJ-COF and the building units. (b) Experimental and simulated XRD patterns of DvDf-C3XJ-COF. (c) The lattice parameters and space groups of DvDf-C3XJ-COF. C, grey; N, blue; O, red. H atoms are omitted for clarity. (d) N_2 adsorption–desorption isotherms of DvDf-C3XJ-COF (inset: pore size distribution).

Previous reports indicate that hydrazone-linked COFs exhibit excellent optical performance.[10a,13] Notably, when an oxygen atom is positioned *ortho* to the acylhydrazone, the hydrogen bonds formed between the N, O, and H atoms enhance the degree of π-conjugation in the COFs, leading to increased fluorescence intensity. Fig. S3 (ESI†) presents the UV/Vis absorption spectra of DvDf-C3XJ-COF, the monomer DvDf, and C3XJOPr. In the solid state, DvDf-C3XJ-COF shows a pronounced UV absorption band around 405 nm, which is redshifted compared to its structural monomers. This shift is attributed to the presence of extended π-conjugation within the DvDf-C3XJ-COF framework. The fluorescence properties of DvDf-C3XJ-COF were then investigated. When dispersed in various solvents, all DvDf-C3XJ-COF solutions exhibit strong fluorescence emission (Fig. S4, ESI†).

The side walls of DvDf-C3XJ-COF are rich in nitrogen and oxygen atoms, by which the chelating sites created can effectively bind to metal ions,[14] thus facilitating rapid fluorescence detection. Upon adding mercury ions to the DvDf-C3XJ-COF solutions, the fluorescence intensity of the original DvDf-C3XJ-COF solutions decreased obviously (Fig. S5, ESI†). To investigate the fluorescence

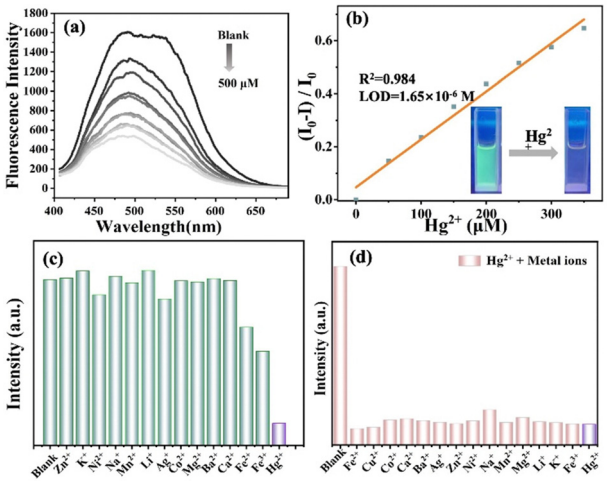

Fig. 2 (a) The fluorescence emission spectrum of DvDf-C3XJ-COF dispersed in EtOH : H_2O = 1 : 1 with the addition of different amounts of Hg^{2+} (0 to 500 μM). (b) The linear relationship between the fluorescence intensity of DvDf-C3XJ-COF with the concentration of Hg^{2+} (Inset: A photograph demonstrating the fluorescence change of DvDf-C3XJ-COF in EtOH : H_2O = 1 : 1 following the addition of 300 μM Hg^{2+}, illuminated under a UV lamp with λ_{ex} = 365 nm). (c) The fluorescence intensity ratio of DvDf-C3XJ-COF in the presence of different metal ions (300 μM). (d) The fluorescence intensity ratio of DvDf-C3XJ-COF + Hg^{2+} in the presence of different metal ions (300 μM).

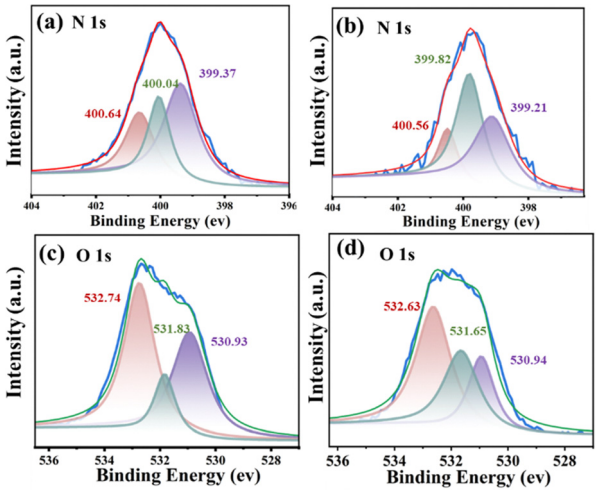

Fig. 3 High-resolution N 1s XPS spectrum of (a) DvDf-C3XJ-COF and (b) DvDf-C3XJ-COF + Hg^{2+}. High-resolution O 1s XPS spectrum of (c) DvDf-C3XJ-COF and (d) DvDf-C3XJ-COF + Hg^{2+}.

quenching phenomenon in response to Hg^{2+} ions, the solutions with varying Hg^{2+} concentrations were prepared and added to the DvDf-C3XJ-COF suspensions, followed by fluorescence spectroscopy analysis. As illustrated in Fig. 2a, the fluorescence intensity of the DvDf-C3XJ-COF decreased progressively with increasing concentrations of Hg^{2+} ions. Almost 400 μM Hg^{2+} ions resulted in nearly 65% quenching of the original fluorescence. Fig. 2b demonstrates that the fluorescence quenching of DvDf-C3XJ-COF by Hg^{2+} aligns well with the Stern–Volmer equation within the Hg^{2+} concentration range from 5 to 350 μM. The limit of detection (LOD) for Hg^{2+} using the DvDf-C3XJ-COF was determined to be 1.65 × 10^{-6} M, calculated by the formula LOD = 3 Sd/k (where Sd represents the standard deviation of the fluorescence intensity of DvDf-C3XJ-COF and k is the slope of the calibration curve), based on a strong linear correlation (R^2 = 0.984, Fig. 3b). The LOD of DvDf-C3XJ-COF is comparable to that of previously reported probes (Table S2, ESI†), but it offers a wider linear detection range. This means that DvDf-C3XJ-COF can not only detect very low concentrations of Hg^{2+} but also maintain a linear response over a broader concentration range, thereby enhancing the accuracy and reliability of detection.

To evaluate the selectivity of DvDf-C3XJ-COF for Hg^{2+} ions, we examined the impact of other metal ions on its fluorescence. A concentration of 300 μM of various metal ions (Zn^{2+}, K^+, Ni^{2+}, Na^+, Mn^{2+}, Li^+, Ag^+, Co^{2+}, Mg^{2+}, Ba^{2+}, Ca^{2+}, Fe^{2+}, Fe^{3+} ions) was added to the DvDf-C3XJ-COF suspension, and these ions produced only minor effects on the fluorescence emission of DvDf-C3XJ-COF (Fig. 2c). In contrast, the fluorescence intensity of DvDf-C3XJ-COF was significantly quenched upon the introduction of Hg^{2+} ions. These findings indicate that DvDf-C3XJ-COF exhibits a high selectivity for Hg^{2+} ions. To rule out potential interference from other ions, competitive experiments were performed to confirm the high selectivity of DvDf-C3XJ-COF. The fluorescence intensity of DvDf-C3XJ-COF suspensions with 300 μM Hg^{2+} ions was measured both before and after introducing various other metal ions (300 μM). As shown in Fig. S6 (ESI†) and Fig. 2d, the fluorescence quenching efficiency of Hg^{2+} on DvDf-C3XJ-COF remained unchanged. Basically, even in the presence of mixed metal ions. These results demonstrate that DvDf-C3XJ-COF can act as a highly selective fluorescent probe for detecting Hg^{2+} ions.

To investigate the quenching mechanism, X-ray photoelectron spectroscopy (XPS) analysis was conducted on both the DvDf-C3XJ-COF and the sample quenched by Hg^{2+} ions. The composition of the elements is shown in Fig. S7 and S8 (ESI†). The key peaks observed for DvDf-C3XJ-COF and DvDf-C3XJ-COF + Hg^{2+} were identified as C 1s, O 1s, and N 1s, confirming the successful formation of hydrazone bonds. In addition, the presence of an extra peak corresponding to the Hg 4f state in the DvDf-C3XJ-COF + Hg^{2+} sample verified that Hg was effectively incorporated into the COF structure. By analyzing the deconvoluted N 1s spectra of both DvDf-C3XJ-COF and DvDf-C3XJ-COF + Hg^{2+}, the characteristic peaks of DvDf-C3XJ-COF all shifted to lower values, likely indicating the presence of coordination interactions within the structure (Fig. 3a and b).

Furthermore, a comparison of the high-resolution O 1s XPS spectra between DvDf-C3XJ-COF and DvDf-C3XJ-COF + Hg^{2+} revealed slight shifts in the characteristic peaks, which can be attributed to changes in electron cloud density caused by Hg incorporation (Fig. 3c and d). These findings confirmed the successful integration of Hg ions into the DvDf-C3XJ-COF framework through electrostatic and coordination bonding. The fluorescence lifetimes of both DvDf-C3XJ-COF and DvDf-C3XJ-COF + Hg^{2+} were also measured. The fluorescence lifetime of DvDf-C3XJ-COF was found to be 1.57 ns, while that of DvDf-C3XJ-COF + Hg^{2+} was 1.42 ns, indicating that the quenching

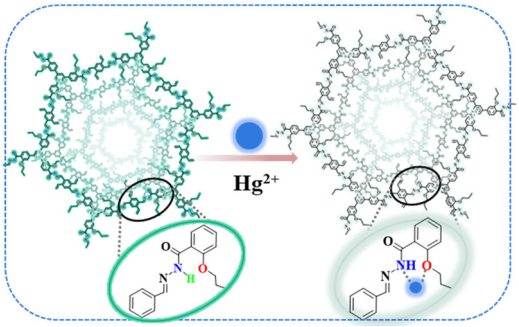

Fig. 4 Proposed mechanism of DvDf-C3XJ-COF for the detection of Hg^{2+}.

of DvDf-C3XJ-COF fluorescence by Hg^{2+} occurs through a dynamic quenching mechanism (Fig. S9, ESI†). Based on the above findings, a potential mechanism for the quenching of DvDf-C3XJ-COF fluorescence was proposed (Fig. 4). The hydrogen bonds in DvDf-C3XJ-COF contribute to the formation of an extensive conjugated system, which is responsible for its strong fluorescence properties.[15] However, upon the introduction of Hg^{2+} ions, these hydrogen bonds are disrupted due to the coordination interactions with the metal ions. Specifically, the oxygen atom in the alkoxy group and the secondary amine group bind with the Hg^{2+} ions. This coordination leads to the quenching of the fluorescence, as the structural changes induced by Hg^{2+} ions break down the conjugation within the COF, suppressing its luminescent properties.

In summary, a hydrazone-linked COF, DvDf-C3XJ-COF, was successfully synthesized through Schiff base condensation. The hydrazone linkage, along with hydrogen bond support, provides DvDf-C3XJ-COF with excellent chemical stability, high crystallinity, and strong fluorescence. Moreover, DvDf-C3XJ-COF exhibits high selectivity and sensitivity towards Hg^{2+} ions, with a detection limit as low as 1.65×10^{-6} M. The fluorescence quenching mechanism for Hg^{2+} ions is attributed to coordination interactions, occurring through a dynamic quenching process. This study not only offers a novel approach for constructing fluorescent COFs and expands the structural variety of COFs, but also opens new avenues for designing fluorescent DvDf-C3XJ-COF probes for detecting heavy metal ions.

This work was supported by the Natural Science Foundation of Shandong Province (ZR2021MB067 and ZR2019PB002), the National Natural Science Foundation of China (51603114), and the Doctoral Fund of Qingdao Agriculture University (663-1115046, 663-1117016, and 665-1120048). D. C. also thanks the support from Jiangxi Double Thousand Plan.

Data availability

The data supporting this article have been included as part of the ESI.†

Conflicts of interest

There are no conflicts to declare.

Notes and references

1 (*a*) W. C. Li and H. F. Tse, *Environ. Sci. Pollut. Res. Int.*, 2015, **22**, 192; (*b*) E. M. Nolan and S. J. Lippard, *Chem. Rev.*, 2008, **108**, 3443; (*c*) S. J. Spiegel, *Lancet*, 2017, **390**, 226.
2 (*a*) X. Wang, Z. Jiang, C. Yang, S. Zhen, C. Huang and Y. Li, *J. Hazard. Mater.*, 2022, **423**, 126978; (*b*) J. Qi, B. Li, X. Wang, Z. Zhang, Z. Wang, J. Han and L. Chen, *Sens. Actuators, B*, 2017, **251**, 224; (*c*) M. Li, Q. Shi, N. Song, Y. Xiao, L. Wang, Z. Chen and T. D. James, *Chem. Soc. Rev.*, 2023, **52**, 5827.
3 (*a*) T. Gong, J. Liu, X. Liu, J. Liu, J. Xiang and Y. Wu, *Food Chem.*, 2016, **213**, 306; (*b*) H. Wang, Z. Wu, B. Chen, M. He and B. Hu, *Analyst*, 2015, **140**, 5619; (*c*) T. Rasheed, C. Li, L. Fu, F. Nabeel, C. Yu, L. Gong and Y. Zhou, *J. Mol. Liq.*, 2018, **272**, 440; (*d*) D. Dai, J. Yang, Y. Wang and Y. W. Yang, *Adv. Funct. Mater.*, 2020, **31**, 2006168.
4 (*a*) X. Feng, X. Ding and D. Jiang, *Chem. Soc. Rev.*, 2012, **41**, 6010; (*b*) A. P. Côté, A. I. Benin, N. W. Ockwig, M. O'Keeffe, A. J. Matzger and O. M. Yaghi, *Science*, 2005, **310**, 1166.
5 (*a*) S.-Y. Ding and W. Wang, *Chem. Soc. Rev.*, 2013, **42**, 548; (*b*) N. A. Rejali, M. Dinari and Y. Wang, *Chem. Commun.*, 2023, **59**, 11631; (*c*) W.-R. Cui, W. Jiang, C.-R. Zhang, R.-P. Liang, J. Liu and J.-D. Qiu, *ACS Sustainable Chem. Eng.*, 2020, **8**, 445.
6 (*a*) C. Gong, C. Yan, J. Liu, J. Li, J. Fu, C. Chen, Y. Huang, G. Yuan and Y. Peng, *TrAC-Trend Anal. Chem.*, 2024, **173**, 117625; (*b*) X. L. Mao, Y. J. Cai, Q. X. Luo, X. Liu, Q. Q. Jiang, C. R. Zhang, L. Zhang, R. P. Liang and J. D. Qiu, *Anal. Chem.*, 2024, **96**, 5037; (*c*) W.-R. Cui, C.-R. Zhang, W. Jiang, F.-F. Li, R.-P. Liang, J. Liu and J.-D. Qiu, *Nat. Commun.*, 2020, **11**, 436; (*d*) Y. Yang, C. Zhang, D. Cao, Y. Song, S. Chen, Y. Song, F. Wang, G. Wang and Y. Yuan, *Chem. Commun.*, 2024, **60**, 2605; (*e*) S. Wang, H. Li, H. Huang, X. Cao, X. Chen and D. Cao, *Chem. Soc. Rev.*, 2022, **51**, 2031.
7 (*a*) L. Y. L. Zhang, Z.-J. Sun and H. Deng, *Aggregate*, 2021, **2**, e24; (*b*) X.-R. Chen, C.-R. Zhang, X. Liu, R.-P. Liang and J.-D. Qiu, *Chem. Commun.*, 2023, **59**, 9521.
8 S. Y. Ding, M. Dong, Y. W. Wang, Y. T. Chen, H. Z. Wang, C. Y. Su and W. Wang, *J. Am. Chem. Soc.*, 2016, **138**, 3031.
9 A. C. Pratt, *Chem. Soc. Rev.*, 1977, **6**, 63.
10 (*a*) Z. Li, K. Geng, T. He, K. T. Tan, N. Huang, Q. Jiang, Y. Nagao and D. Jiang, *Angew. Chem., Int. Ed.*, 2021, **60**, 19419; (*b*) M. Yuan, F. Ma, L. Chen, B. Li, X. Dai, J. Shu, L. He, J. Chen, S. Lin, G. Xie, Z. Chai and S. Wang, *J. Am. Chem. Soc.*, 2024, **146**, 1250; (*c*) Y. Nailwal, M. A. Addicoat, M. Gaurav and S. K. Pal, *ACS Appl. Nano Mater.*, 2023, **6**, 1714; (*d*) S. Zhou, X. Wang, X. Cao, J. Ning and L. Hao, *Chem. Commun.*, 2022, **58**, 12240.
11 C. Peng, L. Pei, S. Chen, Y. Song and L. Wang, *J. Electroanal. Chem.*, 2023, **934**, 117307.
12 F. J. Uribe-Romo, C. J. Doonan, H. Furukawa, K. Oisaki and O. M. Yaghi, *J. Am. Chem. Soc.*, 2011, **133**, 11478.
13 H. Zhuang, C. Guo, J. Huang, L. Wang, Z. Zheng, H. N. Wang, Y. Chen and Y. Q. Lan, *Angew. Chem., Int. Ed.*, 2024, **63**, e202404941.
14 (*a*) M. R. Jalali Sarvestani, T. Madrakian and A. Afkhami, *Food Chem.*, 2023, **402**, 134246; (*b*) Y. He, X. Wang, K. Wang and L. Wang, *Dyes Pigments*, 2020, **173**, 107880.
15 X. Li, Q. Gao, J. Wang, Y. Chen, Z.-H. Chen, H.-S. Xu, W. Tang, K. Leng, G.-H. Ning, J. Wu, Q.-H. Xu, S. Y. Quek, Y. Lu and K. P. Loh, *Nat. Commun.*, 2018, **9**, 2335.

